ELSEVIER

Chemical Engineering Journal 125 (2007) 149–163

Chemical Engineering Journal

www.elsevier.com/locate/cej

Design of a gas distributor: Three-dimensional CFD simulation of a coupled system consisting of a gas chamber and a bubble column

M.T. Dhotre, J.B. Joshi *

Institute of Chemical Technology, University of Mumbai, Matunga, Mumbai 400019, India

Received 12 February 2006; received in revised form 28 August 2006; accepted 28 August 2006

Abstract

CFD simulation for bubble column and a large number of chamber configurations have been carried out. The numerical simulations were based on a two-fluid k–ε model. An attempt has been made to simulate the flow pattern on the upstream and downstream of the distributor and its effect on performance of the bubble column. A procedure has been proposed for connecting the gas chamber to bubble column reactor. The extreme cases of uniform and mal-distribution were considered and the effect of mal-distribution was investigated on the flow pattern in the bubble column. The effects of opening area and hole diameter were investigated in the range of 0.64–4% and 2–4 mm, respectively. The effect of inlet nozzle size and its location with respect to the distributor were found to be very important. The flow pattern within the gas chamber has been comprehensively analyzed and the velocities through all the holes have been estimated for assessing the uniformity of the gas distribution. It was found that, the chamber configuration has an effect on the uniformity of gas distribution particularly in the sparger region of bubble column reactors. The uniformity of gas distribution was found to increase with an increase in the distributor pressure drop and a decrease in the inlet kinetic head of the gas. Recommendations have been made for the inlet nozzle size and its location, opening area and hole diameter. Further, the development of hold-up profile and its significance on design parameters have been explored. From the quantitative information reported in this paper, it may be possible to select the design parameters of distributor and gas chamber depending upon the desired level of uniformity of distribution and for a given bubble column in terms of diameter (D), height of dispersion (H_D), superficial gas (V_G) and liquid velocity (V_L).

Keywords: Bubble column; Gas chamber; CFD; Distributor design

1. Introduction

Bubble column reactors find a widespread applications in the chemical industry due to their simple construction and operation. These columns are characterized by intense liquid circulation, which provides a good degree of liquid phase mixing, heat and mass transfer rates between the fluids and the column wall. Important applications include oxidation, hydrogenation, hydrohalogenation, ammonolysis, hydroformylation, Fischer–Tropsch reaction, ozonolysis, carbonylation, carboxylation, alkylation, fermentation, waste water treatment, hydrometallurgical operation, steel ladle stirring, column flotation, etc.

A bubble column consists of a vertical cylindrical vessel with height-to-diameter ratio in the range of 1–20 (more commonly 3–10). Gas is introduced at the bottom via a sparger. Several designs of the sparger are used in practice, which include: sieve plate, ring, spider, radial sparger, ejector, injector, etc. One of the most important features in the design and operation of a bubble column is an appropriate selection of the gas-distributing element. The sparger or distributor governs the bubble size distribution and the hold-up profile particularly in the transverse direction. These in turn decide the flow pattern, effective interfacial area, rates of mass transfer, heat transfer and mixing. The mal-distribution reduces the effectiveness of the gas–liquid contacting and may result into dead zones or sparge-hole plugging, and as an extreme case weeping through part of the distributor. All these non-ideal flow behaviors have profound impact on the residence time distribution and the reactor performance particularly when selectivity and quality are important.

A good distributor should introduce bubbles and distribute them uniformly over the entire cross-section and this objective needs to be achieved with as minimum a pressure drop as possible. In order to obtain uniform distribution, it is important to understand the flow pattern on the upstream and downstream

* Corresponding author. Tel.: +91 22 414 5616; fax: +91 22 414 5614.
E-mail address: jbj@udct.org (J.B. Joshi).

1385-8947/$ – see front matter © 2006 Elsevier B.V. All rights reserved.
doi:10.1016/j.cej.2006.08.027

Nomenclature

a	interfacial area (m^{-1})
C_B	interface energy transfer factor
C_D	drag coefficient ($kg\,m^{-3}\,s^{-1}$)
CFD	computational fluid dynamics
C_L	lift force coefficient
C_V	virtual mass force coefficient
C_0, C_1	drift-flux constant
$C_{\varepsilon 1}$, $C_{\varepsilon 2}$, C_μ	constant in turbulence models
d_B	bubble diameter (m)
d_0	orifice or hole diameter (m)
D	diameter of the column (m)
D_L	axial dispersion coefficient ($m^2\,s^{-1}$)
D_N	nozzle size (m)
E_I	net energy input (W)
f_{DZ}	drag force on single bubble ($N\,m^{-3}$)
F_{DR}	frictional force in the radial direction per unit volume of dispersion ($N\,m^{-3}$)
F_{DZ}	frictional force in the axial direction per unit volume of dispersion ($N\,m^{-3}$)
$F_{D\theta}$	frictional force in the tangential direction per unit volume of dispersion ($N\,m^{-3}$)
F_{LR}	lift force per unit volume of dispersion ($N\,m^{-3}$)
$F_{L\theta}$	lift force in the tangential direction per unit volume of dispersion ($N\,m^{-3}$)
F_{VR}	radial virtual mass force per unit volume of dispersion ($N\,m^{-3}$)
F_{VZ}	axial virtual mass force per unit volume of dispersion ($N\,m^{-3}$)
$F_{V\theta}$	tangential virtual mass force per unit volume of dispersion ($N\,m^{-3}$)
g	acceleration due to gravitation ($m\,s^{-2}$)
G	generation term defined in Table 1
H_C	height of chamber (m)
H_D	height of gas dispersion (m)
k	turbulent energy ($m^2\,s^{-2}$)
k_La	mass transfer coefficient (s^{-1})
N	number of holes on the sieve plate distributor
OA	opening area (%)
p	pressure ($N\,m^{-2}$)
P_B	interphase transfer of energy term
ΔP_D	dry pressure drop (Nm^{-2})
ΔP_W	wet pressure drop (Nm^{-2})
r	radial distance (m)
$S_{\phi,k}$	source term in the governing equation
$\mathbf{u}$	axial velocity component ($m\,s^{-1}$)
$\overline{\mathbf{u}_L - \mathbf{u}_G}$	average slip velocity ($m\,s^{-1}$)
$\mathbf{v}$	radial velocity component ($m\,s^{-1}$)
v_B	volume of a bubble (m^3)
$V_{B\infty}$	terminal rise velocity ($m\,s^{-1}$)
V_G	superficial gas velocity ($m\,s^{-1}$)
V_L	superficial liquid velocity ($m\,s^{-1}$)
V_N	nozzle gas velocity ($m\,s^{-1}$)
V_S	axial slip velocity between gas and liquid ($m\,s^{-1}$)
V_{Sr}	radial slip velocity between gas and liquid ($m\,s^{-1}$)
$\mathbf{w}$	tangential velocity component ($m\,s^{-1}$)
y	normal distance from the wall, R–r (m)
z	axial distance along the column (m)

Greek symbols

Γ_K	$\frac{\nu_{t,K}}{\sigma_{\Phi,K}}$
α	molecular thermal diffusivity ($m^2\,s^{-1}$)
ε	turbulent kinetic energy dissipation rate ($m^2\,s^{-3}$)
$\in$	volume fraction
$\in_L$	fractional liquid hold-up at any radial location
$\in_G$	fractional gas hold-up at any radial location
$\bar{\in}_G$	average fractional gas hold-up
$\bar{\in}_L$	average fractional liquid hold-up
ϕ	a time averaged variable
μ	molecular viscosity of phase K (Pa s)
$\mu_{t,K}$	turbulent viscosity of phase K (Pa s)
μ_{eff}	effective turbulent viscosity (Pa s)
τ	stress term ($N\,m^{-2}$)
ν	molecular kinematic viscosity of liquid ($m^2\,s^{-1}$)
ν_t	turbulent kinematic viscosity of liquid ($m^2\,s^{-1}$)
θ_{mix}	mixing time (s)
ρ	density ($kg\,m^{-3}$)
ρ_D	average density of gas–liquid dispersion ($\bar{\in}_L\rho_L + \bar{\in}_G\rho_G$) ($kg\,m^{-3}$)
ρ_G	density of gas ($kg\,m^{-3}$)
ρ_L	density of liquid ($kg\,m^{-3}$)
σ	surface tension of liquid (N m)
σ_ϕ	turbulent Prandtl number for momentum transfer
σ_ε	turbulent Prandtl number for kinetic energy dissipation rate
σ_f	turbulent Prandtl number for bubble motion or dispersion number
σ_k	turbulent Prandtl number for turbulent kinetic energy

Subscripts

G	gas phase
K	phase, K = G: gas phase, K = L: liquid phase
L	liquid phase
lam	laminar

sides of the distributor. Velocity distribution of gas through sparger holes strongly depends on the design of gas chamber. The design parameters include the aspect ratio, inlet nozzle position and its size, in addition, if the sparger is of sieve plate type then opening area of the gas distributor, number of holes and their spatial distribution. The gas distributor performance also depends upon the pressure field and the flow pattern on the downstream face of the distributor, which depends upon the column diameter, superficial gas velocity and the distributor design itself. Thus, for the design of gas–liquid reactors such as bubble columns, the distributor design should take into account the flow pattern on the both sides as well as through the distributor holes. Despite its

importance, there are no generally accepted procedures for the proper design of a gas–liquid distributor and are largely empirical and based on conflicting "rules of thumb". For instance, often the pressure drop across the distributor is used as the criterion for design, and one of the recommendations is that the pressure drop across the distributor should be 10–30% of the static head of the multiphase dispersion (Kunii and Levenspiel [1]). Clearly the use of this criterion is not satisfactory, as the same may be obtained for instance from two distributors, one with a single hole and another with a large number of smaller holes. Conversely, nor it is sufficient to specify only the opening area on the plate. The substitution of a large number of small holes for a smaller number of large holes may leave the proportion of opening area unchanged but will significantly alter the pressure drop and flow pattern. Dhotre and Joshi [2] analyzed the flow pattern in the gas chamber using CFD and proposed a procedure for sparger design. This work assumed uniform pressure distribution on the downstream side of the sparger or at the bottom of the gas–liquid dispersion in a column. Since the real column operation is characterized by intense liquid circulation with concomitant pressure distribution, it was thought desirable to extend the work of Dhotre and Joshi [2] and undertake the CFD simulation of the bubble column together with gas chamber so that the actual pressure profiles on both sides of the sparger get included in the analysis. An attempt has been made to understand the various combinations of sieve plate as sparger (d_0, OA, N), bubble column (D, H_D and V_G) and gas chamber (aspect ratio, location and diameter of inlet nozzle). The results are expected to be useful for the sparger design.

2. Mathematical model

2.1. Gas chamber

The analysis of the gas chamber below a distributor plate involves single-phase three-dimensional complex turbulent flow. The continuity and momentum equations can be written in the following form:

2.1.1. Continuity equation

$$\nabla(\rho \mathbf{u}) = 0 \tag{1}$$

2.1.2. Momentum equation

$$\nabla(\rho \mathbf{u}\mathbf{u}) = -\nabla p + \nabla\tau + \rho g, \tag{2}$$

The terms on the right hand side of Eq. (2) are, respectively, representing the pressure gradient, stress and gravity. The effective turbulent viscosity (μ_{eff}) was computed from a velocity scale ($k^{1/2}$) and a length scale $k^{3/2}/\varepsilon$ which were predicted at each point in the flow via the solution of the following transport equations for k and ε:

$$\nabla(\rho \mathbf{u}k) = -\nabla\left(\frac{\mu_{\text{eff}}}{\sigma_k}\nabla k\right) + G - \rho\varepsilon \tag{3}$$

$$\nabla(\rho \mathbf{u}\varepsilon) = \nabla\left(\frac{\mu_{\text{eff}}}{\sigma_\varepsilon}\nabla\varepsilon\right) + C_{\varepsilon 1}\frac{\varepsilon}{k}G - C_{\varepsilon 2}\,\rho\frac{\varepsilon^2}{k} \tag{4}$$

The turbulent viscosity is then related to k and ε by the expression:

$$\mu_{\text{eff}} = \mu + C_\mu \rho \frac{k^2}{\varepsilon}, \tag{5}$$

The coefficients $C_{\varepsilon 1}$, $C_{\varepsilon 2}$, C_μ, σ_k, σ_ε are the k–ε model parameters and the following values were selected: $C_{\varepsilon 1} = 1.44$, $C_{\varepsilon 2} = 1.92$, $C_\mu = 0.09$, $\sigma_k = 1.0$, $\sigma_\varepsilon = 1.3$. The term G in Eqs. (3) and (4) is the production of turbulent kinetic energy and described by $\tau{:}\nabla\mathbf{u}$ where $\tau = -\mu_{\text{eff}}[\nabla\mathbf{u} + (\nabla\mathbf{u})^{\text{T}}]$.

2.2. Bubble column

The gas–liquid flow in bubble column is inherently unsteady and comprised of various flow processes occurring at different length and time scales. As far as the steady and averaged profiles of variables are concerned, flow can be represented by the steady state model. The equations of continuity and motion for the three-dimensional cylindrical co-ordinate system can be represented in the following generalized form (Stewart and Wendroff [3]; Jakobsen et al. [4]; Joshi [5])

$$\begin{aligned}\frac{1}{r}\frac{\partial}{\partial r}(r \in \rho \mathbf{v}\Phi)_{\text{K}} + \frac{\partial}{\partial z}(\in \rho \mathbf{u}\Phi)_{\text{K}} + \frac{1}{r}\frac{\partial}{\partial \theta}(\in \rho \mathbf{w}\Phi)_{\text{K}} \\ = \frac{\partial}{\partial r}\left(\frac{1}{r}\frac{\partial}{\partial r}(r\Gamma \in \Phi)\right)_{\text{K}} + \frac{\partial^2}{\partial z^2}(\in \Gamma\Phi)_{\text{K}} \\ + \frac{1}{r^2}\frac{\partial^2}{\partial \theta^2}(\in \Gamma\Phi)_{\text{K}} + S_{\Phi\text{K}}\end{aligned} \tag{6}$$

where Φ is any transport variable, K denotes the phase [K = G or L] S_Φ is the source term for the respective dependent variable. Values of Φ and S_Φ for different transport variables have been given in Table 1 and Γ_{K} is effective turbulent diffusivity, $\Gamma_k = (\nu_{t,\text{K}}/\sigma_{\phi,\text{K}})$, where the turbulent eddy diffusivity for liquid phase is given as:

$$\nu_{\text{t,L}} = \nu_{\text{L lam}} + \frac{C_\mu k^2}{\varepsilon} \tag{7}$$

where k is turbulent kinetic energy and ε is turbulent kinetic energy dissipation rate in liquid phase. The eddy diffusivity for gas phase was estimated from the knowledge of eddy diffusivity of liquid phase. The modeled form of the liquid phase k and ε transport equation are given in Table 1. From Table 1, it can be seen that most of the terms are derived from gas and liquid velocities. In addition, in two-phase flows, momentum and energy transfer occurs across the interface. Therefore, the drag force (F_{DZ}, F_{DR} and $F_{\text{D}\theta}$), virtual mass force (F_{VZ}, F_{VR}, $F_{\text{V}\theta}$), and lift force (F_{LR} and $F_{\text{L}\theta}$) appear in the axial, radial and tangential components of the momentum balance (Table 1). Furthermore, the interphase transfer of energy (P_{B}) appears in the equations for turbulent kinetic energy and turbulent energy dissipation rates.

3. Boundary conditions

In order to obtain a well-posed system of equations, reasonable boundary conditions for the computational domain have to be implemented. Fig. 1 shows the computational setup of

Table 1
Governing equation for bubble column

	Φ	σ_Φ	σ_f	$S_{\Phi,\mathrm{K}}$= source terms
The governing equations written in a general form: $\frac{1}{r}\frac{\partial}{\partial r}(r\in\rho\mathbf{v}\Phi)_\mathrm{K}+\frac{\partial}{\partial z}(\in\rho\mathbf{u}\Phi)_\mathrm{K}+\frac{1}{r}\frac{\partial}{\partial\theta}(\in\rho\mathbf{w}\Phi)_\mathrm{K}=$ $\frac{1}{r}\frac{\partial}{\partial r}\left(r\in\Gamma\frac{\partial\Phi}{\partial r}\right)_\mathrm{K}+\frac{\partial}{\partial z}\left(\in\Gamma\frac{\partial\Phi}{\partial z}\right)_\mathrm{K}+\frac{1}{r^2}\frac{\partial}{\partial\theta}\left(\in\Gamma\frac{\partial\Phi}{\partial\theta}\right)_\mathrm{K}+S_{\Phi,\mathrm{K}}$				
Conservation of mass	1	∞	1 to ∞	$\frac{1}{r}\frac{\partial}{\partial r}\left(r\frac{\mu_{t,\mathrm{K}}}{\sigma_f}\frac{\partial\in_\mathrm{K}}{\partial r}\right)+\frac{\partial}{\partial z}\left(\frac{\mu_{t,\mathrm{K}}}{\sigma_f}\frac{\partial\in_\mathrm{K}}{\partial z}\right)+\frac{1}{r^2}\frac{\partial}{\partial\theta}\left(\frac{\mu_{t,\mathrm{K}}}{\sigma_f}\frac{\partial\in_\mathrm{K}}{\partial\theta}\right)$
Conservation of axial velocity momentum	$\mathbf{u}$	1.0	1 to ∞	$-\in_\mathrm{K}\frac{\partial P}{\partial z}+\in_\mathrm{K}\rho_\mathrm{K}g\pm F^*_{\mathrm{DZ}}\in_\mathrm{L}\pm F^*_{\mathrm{VZ}}\in_\mathrm{L}+$ $\left(\frac{1}{r}\frac{\partial}{\partial r}\left(r\in\mu_t\frac{\partial\mathbf{v}}{\partial z}\right)+\frac{\partial}{\partial z}\left(\in\mu_t\frac{\partial\mathbf{u}}{\partial z}\right)+\frac{1}{r}\frac{\partial}{\partial\theta}\left(\in\mu_t\frac{\partial\mathbf{w}}{\partial z}\right)\right)_\mathrm{K}+$ $\mathbf{u}_\mathrm{K}\left(\frac{1}{r}\frac{\partial}{\partial r}\left(r\frac{\mu_t}{\sigma_f}\frac{\partial\in}{\partial r}\right)+\frac{\partial}{\partial z}\left(\frac{\mu_t}{\sigma_f}\frac{\partial\in}{\partial z}\right)+\frac{1}{r^2}\frac{\partial}{\partial\theta}\left(\frac{\mu_t}{\sigma_f}\frac{\partial\in}{\partial\theta}\right)\right)_\mathrm{K}+$ $\left(\frac{\mu_t}{\sigma_f}\frac{\partial\in}{\partial z}\right)_\mathrm{K}\left(\frac{1}{r}\frac{\partial}{\partial r}(r\mathbf{v})+\frac{\partial u}{\partial z}+\frac{1}{r}\frac{\partial\mathbf{w}}{\partial\theta}\right)_\mathrm{K}$
Conservation of radial velocity momentum	$\mathbf{v}$	1.0	1 to ∞	$-\in_\mathrm{K}\frac{\partial P}{\partial r}\pm F^*_{\mathrm{DR}}\in_\mathrm{L}\pm F^*_{\mathrm{VR}}\in_\mathrm{L}\pm F^*_{\mathrm{LR}}\in_\mathrm{L}+$ $\left(\frac{1}{r}\frac{\partial}{\partial r}\left(r\in\mu_t\frac{\partial\mathbf{v}}{\partial r}\right)+\frac{\partial}{\partial z}\left(\in\mu_t\frac{\partial\mathbf{u}}{\partial r}\right)+\frac{1}{r}\frac{\partial}{\partial\theta}\left(\in\mu_t\frac{\partial\mathbf{w}}{\partial r}\right)\right)_\mathrm{K}+$ $\left(\in\frac{\mathbf{w}^2}{r}\right)_\mathrm{K}-\left(2\in\frac{\mu_t}{r^2}\frac{\partial\mathbf{w}}{\partial\theta}\right)_\mathrm{K}-\left(2\in\mu_t\frac{\mathbf{v}}{r^2}\right)_\mathrm{K}+$ $\mathbf{v}_\mathrm{K}\left(\frac{1}{r}\frac{\partial}{\partial r}\left(r\frac{\mu_t}{\sigma_f}\frac{\partial\in}{\partial r}\right)+\frac{\partial}{\partial z}\left(\frac{\mu_t}{\sigma_f}\frac{\partial\in}{\partial z}\right)+\frac{1}{r^2}\frac{\partial}{\partial\theta}\left(\frac{\mu_t}{\sigma_f}\frac{\partial\in}{\partial\theta}\right)\right)_\mathrm{K}+$ $\left(\frac{\mu_t}{\sigma_f}\frac{\partial\in}{\partial r}\right)_\mathrm{K}\left(\frac{1}{r}\frac{\partial}{\partial r}(r\mathbf{v})+\frac{\partial\mathbf{u}}{\partial z}+\frac{1}{r}\frac{\partial\mathbf{w}}{\partial\theta}\right)_\mathrm{K}$
Conservation of tangential velocity momentum	$\mathbf{w}$	1.0	1 to ∞	$-\in_\mathrm{K}\frac{1}{r}\frac{\partial P}{\partial\theta}\pm F^*_{\mathrm{D}\theta}\in_\mathrm{L}\pm F^*_{\mathrm{V}\theta}\in_\mathrm{L}\pm F^*_{\mathrm{L}\theta}\in_\mathrm{L}+$ $\left(\frac{1}{r}\frac{\partial}{\partial r}\left(r\in\mu_t\frac{\partial\mathbf{v}}{\partial\theta}\right)+\frac{\partial}{\partial z}\left(\in\mu_t\frac{\partial\mathbf{u}}{\partial\theta}\right)+\frac{1}{r^2}\frac{\partial}{\partial\theta}\left(\in\mu_t\frac{\partial\mathbf{w}}{\partial\theta}\right)\right)_\mathrm{K}-$ $\left(\in\frac{\mathbf{vw}}{r}\right)_\mathrm{K}+\left(\in\frac{\mu_t}{r^2}\frac{\partial\mathbf{v}}{\partial\theta}\right)_\mathrm{K}-\left(\frac{1}{r}\frac{\partial}{\partial\theta}\left(2\in\mu_t\frac{\mathbf{v}}{r}\right)\right)_\mathrm{K}+$ $\mathbf{w}_\mathrm{K}\left(\frac{1}{r}\frac{\partial}{\partial r}\left(r\frac{\mu_t}{\sigma_f}\frac{\partial\in}{\partial r}\right)+\frac{\partial}{\partial z}\left(\frac{\mu_t}{\sigma_f}\frac{\partial\in}{\partial z}\right)+\frac{1}{r^2}\frac{\partial}{\partial\theta}\left(\frac{\mu_t}{\sigma_f}\frac{\partial\in}{\partial\theta}\right)\right)_\mathrm{K}+$ $\left(\frac{\mu_t}{\sigma_f}\frac{\partial\in}{\partial\theta}\right)_\mathrm{K}\left(\frac{1}{r}\frac{\partial}{\partial r}(r\mathbf{v})+\frac{\partial\mathbf{u}}{\partial z}+\frac{1}{r}\frac{\partial\mathbf{w}}{\partial\theta}\right)_\mathrm{K}$
Conservation of turbulent kinetic energy	k	1.0	-	$\in_\mathrm{L}(G+P_\mathrm{B}-\rho_\mathrm{L}\varepsilon)$
Conservation of turbulent energy dissipation	ε	1.3	-	$\in_\mathrm{L}\frac{\varepsilon}{k}(C_{\varepsilon1}(G+P_\mathrm{B})-C_{\varepsilon2}\rho_\mathrm{L}\varepsilon)$

$P_\mathrm{B}=C_\mathrm{B}(F_{\mathrm{DR}}V_\mathrm{S}+F_{\mathrm{DZ}}V_\mathrm{S}+F_{\mathrm{D}\theta}V_\mathrm{S});\quad F_{\mathrm{LR}}=-C_\mathrm{L}\in_\mathrm{G}\rho_\mathrm{L}(\mathbf{u}_\mathrm{G}-\mathbf{u}_\mathrm{L})\frac{\partial\mathbf{u}_\mathrm{L}}{\partial r};\quad F_{\mathrm{L}\theta}=-C_\mathrm{L}\in_\mathrm{G}\rho_\mathrm{L}\frac{(\mathbf{w}_\mathrm{G}-\mathbf{w}_\mathrm{L})}{r}\frac{\partial\mathbf{w}_\mathrm{L}}{\partial\theta}$

$F_{\mathrm{VZ}}=-C_\mathrm{V}\in_\mathrm{G}\rho_\mathrm{L}\left\{\frac{\partial}{\partial r}(\mathbf{v}_\mathrm{G}-\mathbf{v}_\mathrm{L})+\frac{\partial}{\partial z}(\mathbf{u}_\mathrm{G}-\mathbf{u}_\mathrm{L})+\frac{1}{r}\frac{\partial}{\partial\theta}(\mathbf{w}_\mathrm{G}-\mathbf{w}_\mathrm{L})\right\};\quad \mathrm{F}_{\mathrm{DZ}}=-\frac{\bar{\in}_\mathrm{G}(\rho_\mathrm{G}-\rho_\mathrm{L})g(\mathbf{u}_\mathrm{G}-\mathbf{u}_\mathrm{L})|\mathbf{u}_\mathrm{G}-\mathbf{u}_\mathrm{L}|}{(\overline{\mathbf{u}_\mathrm{G}-\mathbf{u}_\mathrm{L}})^2}$

$F_{\mathrm{VR}}=-C_\mathrm{V}\in_\mathrm{G}\rho_\mathrm{L}\left(\frac{1}{r}\frac{\partial}{\partial r}r(\mathbf{v}_\mathrm{G}-\mathbf{v}_\mathrm{L})+\frac{\partial}{\partial z}(\mathbf{u}_\mathrm{G}-\mathbf{u}_\mathrm{L})+\frac{1}{r}\frac{\partial}{\partial\theta}(\mathbf{w}_\mathrm{G}-\mathbf{w}_\mathrm{L})\right);\quad F_{\mathrm{DR}}=-\frac{\bar{\in}_\mathrm{G}(\rho_\mathrm{G}-\rho_\mathrm{L})g(\mathbf{v}_\mathrm{G}-\mathbf{v}_\mathrm{L})|\mathbf{v}_\mathrm{G}-\mathbf{v}_\mathrm{L}|}{(\overline{\mathbf{v}_\mathrm{G}-\mathbf{v}_\mathrm{L}})^2}$

$\mathrm{F}_{\mathrm{V}\theta}=-C_\mathrm{V}\in_\mathrm{G}\rho_\mathrm{L}\left(\frac{1}{r}\frac{\partial}{\partial r}r(\mathbf{v}_\mathrm{G}-\mathbf{v}_\mathrm{L})+\frac{\partial}{\partial z}(\mathbf{u}_\mathrm{G}-\mathbf{u}_\mathrm{L})+\frac{1}{r}\frac{\partial}{\partial\theta}(\mathbf{w}_\mathrm{G}-\mathbf{w}_\mathrm{L})\right);\quad F_{\mathrm{D}\theta}=-\frac{\bar{\in}_\mathrm{G}(\rho_\mathrm{G}-\rho_\mathrm{L})g(\mathbf{w}_\mathrm{G}-\mathbf{w}_\mathrm{L})|\mathbf{w}_\mathrm{G}-\mathbf{w}_\mathrm{L}|}{(\overline{\mathbf{w}_\mathrm{G}-\mathbf{w}_\mathrm{L}})^2}$

$G=\mu_{t,\mathrm{L}}\left(2\left(\left\{\frac{\partial\mathbf{v}_\mathrm{L}}{\partial r}\right\}^2+\left\{\frac{1}{r}\frac{\partial\mathbf{w}_\mathrm{L}}{\partial\theta}+\frac{\mathbf{v}_\mathrm{L}}{r}\right\}^2+\left\{\frac{\partial\mathbf{u}_\mathrm{L}}{\partial z}\right\}^2\right)+\left(\frac{\partial\mathbf{v}_\mathrm{L}}{\partial z}+\frac{\partial\mathbf{u}_\mathrm{L}}{\partial r}\right)^2+\left(\frac{1}{r}\frac{\partial\mathbf{u}_\mathrm{L}}{\partial\theta}+\frac{\partial\mathbf{w}_\mathrm{L}}{\partial z}\right)^2+\left(r\frac{\partial}{\partial r}\left(\frac{\mathbf{w}_\mathrm{L}}{r}\right)+\frac{1}{r}\frac{\partial\mathbf{v}_\mathrm{L}}{\partial\theta}\right)^2\right)$

*Force terms are positive for the gas phase and negative for the liquid phase.

both gas chamber and bubble column under consideration. The boundary conditions for the gas chamber and bubble column has been specified as follows.

3.1. Gas chamber

The inlet nozzle was either provided at the bottom or on the side. During simulation, the location and size were varied over a wide range. The top of the gas chamber formed the sieve plate distributor having holes. The holes were distributed in square pitch and pitch to diameter ratio was selected in such a way that no weeping criteria should be satisfied. The holes were uniformly distributed over a square area and then percentage opening area was calculated. The following boundary conditions were employed: (i) at the inlet, the nozzle velocity (V_N) was specified; (ii) at the top surface (distributor), the region of holes, was considered live for the gas flow; (iii) standard wall functions were employed to model the flow near the wall; (iv) for considering connectivity, the pressure profile from downstream of the bubble column was employed on the distributor.

3.2. Bubble column

(i) Along the wall, the velocities satisfy the no-slip boundary conditions (the wall function method based on the log law of the wall is invoked to calculate the wall shear stress and the values of k and ε close to the wall).
(ii) At the inlet, the top surface information obtained from gas chamber was set at inlet holes and a closed part of the distributor was set to no-slip boundary condition.

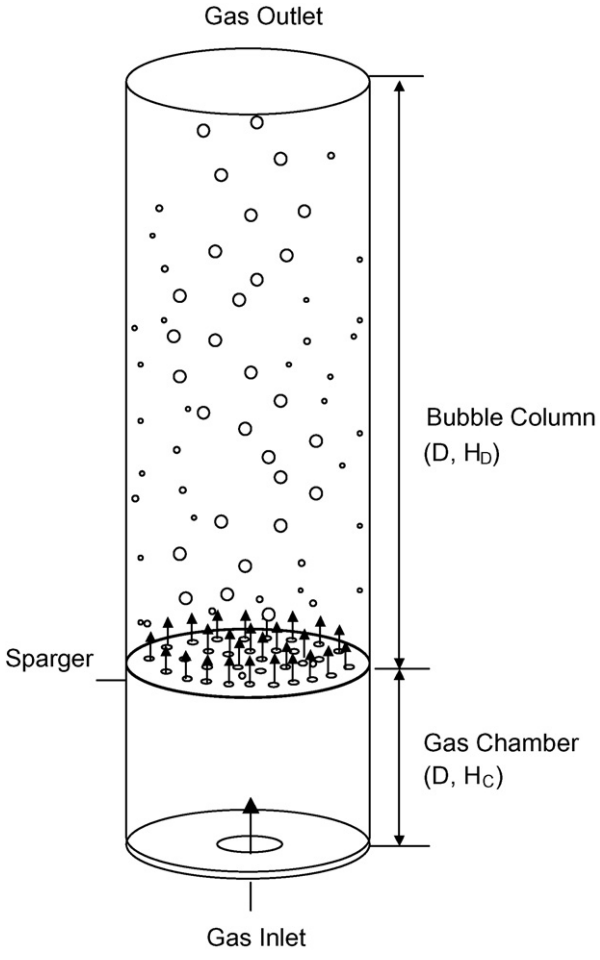

Fig. 1. Schematic of the bubble column reactor and a gas chamber and a bubble column.

(iii) At the top surface of the computational domain, the gradient of the dependent variable are set to zero.

4. Inter-phase force term

The interfacial forces arise due to the momentum transfer across the interface. If the slip velocity is constant, the force is called as drag force. For a single bubble rising in an infinite liquid, the drag force is given by:

$$C_D \frac{\pi}{4} d_B^2 \frac{1}{2} \rho_L (\mathbf{u}_G - \mathbf{u}_L)|\mathbf{u}_G - \mathbf{u}_L| = v_B(\rho_G - \rho_L)g = f_{DZ} \quad (8)$$

The modulus quantity is the slip velocity. The drag force per unit volume of dispersion (F_{DZ}) consisting of N bubbles can be estimated using Eq. (8). On the basis of left hand side of f_{DZ} formulation, F_{DZ} works out to be:

$$F_{DZ} = N f_{DZ} = -\in_G \rho_L \frac{3C_D}{4d_B}(\mathbf{u}_G - \mathbf{u}_L)|\mathbf{u}_G - \mathbf{u}_L| \quad (9)$$

While using Eq. (9) in practice, the knowledge of d_B and slip velocity is needed. The drag force for a single bubble depends on the shape and size of the bubble, nature of the interface and flow around the bubble. The estimation of drag force for a bubble swarm is further complicated by the presence of other surrounding bubbles. Further, the value of C_D is likely to be different for a bubble and a bubble swarm. This is because, the shape and size of a bubble in a bubble swarm is much different from that of an isolated bubble. In addition, the flow structure surrounding a bubble gets modified when it becomes part of a swarm. Further, bubbles do have a size distribution and bubble coalescence and break-up seems to have an important role for correct simulation results. This objective is still under investigation and yet not included in this work. From the foregoing discussion, it is clear that, the use of Eq. (9) is difficult. Alternatively, f_{DZ} and F_{DZ} can be estimated on the basis of right hand side of Eq. (8) as:

$$F_{DZ} = -\in_G(\rho_G - \rho_L)g \quad (10)$$

In a bubble column, the description of drag force should consider the following important real features: (a) the value of slip velocity (V_S) is not constant throughout the column and varies in radial and axial directions. The local value of slip velocity ($\mathbf{u}_G$–$\mathbf{u}_L$) is obtained from the CFD solution and the average V_S can be estimated from the local values. (b) As said earlier, it may be emphasized again that the values of V_S (local and hence average) strongly depend upon the nature of the gas–liquid system. Out of the above two features, the variation of V_S can be included in the F_{DZ} formulation by linearization of Eq. (10) and is given below. The considerations of the feature (b) will be discussed later.

$$F_{DZ} = -\frac{\in_G(\rho_G - \rho_L)g(\mathbf{u}_G - \mathbf{u}_L)}{\overline{(\mathbf{u}_G - \mathbf{u}_L)}} \quad (11)$$

For a typical value of average slip velocity of $0.2\,\mathrm{m\,s^{-1}}$, $\rho_L = 1000\,\mathrm{kg\,m^{-3}}$, $\rho_L \gg \rho_G$, $g = 9.81\,\mathrm{m\,s^{-1}}$, we get:

$$F_{DZ} = C_D \in_G (\mathbf{u}_G - \mathbf{u}_L) \quad (12)$$

where

$$C_D = -\frac{(\rho_G - \rho_L)\,g}{\overline{\mathbf{u}_G - \mathbf{u}_L}} = -\frac{(\rho_G - \rho_L)\,g}{V_S} = 4.9 \times 10^4 \quad (13)$$

It may be pointed out that C_D is not the conventional dimensionless drag coefficient. In this case, it has units of $\mathrm{kg\,m^{-3}\,s^{-1}}$ or $\mathrm{N\,s\,m^{-4}}$. It may be noted that the constant (4.9×10^4) is valid for a fixed value of the slip velocity of $0.2\,\mathrm{m\,s^{-1}}$. If the relative motion is unsteady, a virtual mass force prevails which is additive to the drag force. When the liquid phase flow pattern is non-uniform in the radial direction the rising bubble experiences a radial (or lateral) lift force. In the present work, all the three forces, i.e. drag, lift and virtual mass force have been incorporated with $C_L = 0.1$ and $C_V = 0.5$. Table 1 shows the formulation of these three forces.

5. Energy balance

All the predicted flow patterns must satisfy the energy balance. The rate of energy supply from the gas phase to the liquid phase is given by the following equation:

$$E_I = \frac{\pi}{4} D^2 (\rho_L - \rho_G) g H_D \in_L [V_G + (C_B - 1)\,\bar{\in}_G V_S] \quad (14)$$

When bubbles rise, the pressure energy is converted into turbulent kinetic energy. A fraction of C_B is considered to get transferred to the liquid phase; the rate of energy given by Eq. (14) is finally dissipated in the turbulent liquid motion. We need to establish the energy balance. From CFD simulations, we get the pattern of turbulent energy dissipation rate. Therefore, the predicted energy dissipation rate needs to be equal to the input rate given by Eq. (14). The pertinent detailed discussion has been provided by Dhotre and Joshi [6].

6. Method of solution

The set of steady state governing equations were solved numerically and involved the following steps: (i) generation of suitable grid system; (ii) conversion of governing equation into algebraic equations; (iii) selection of discretization schemes; (iv) formulation of the discretized equation at every grid location; (v) formulation of pressure equation; (vi) development of a suitable iteration scheme for obtaining a final solution. The finite control volume technique of Patankar [7] was employed for the solution of these equations.

6.1. Gas chamber

The equation of continuity and motion were solved (together with the k–ε equations) for getting complete flow pattern in the gas chamber. In our simulations, the finite-volume method in three dimensions was used. The flow in chamber was computed using 54,000–120,000 cells depending upon number of holes and height to diameter ratio and it was found that 12–15 grids per hole were sufficient for resolving the flow. The equations were solved using the SIMPLE algorithm (Patankar [7]). The model equations were solved using a commercial CFD code, FLUENT 6.1 (of Fluent Inc.).

6.2. Bubble column

A power law scheme was used for the discretization of the governing equations for bubble column. A SIMPLE algorithm was used to solve the pressure velocity coupling term. The set of algebraic equations obtained after discretization were solved by Tri-Diagonal Matrix Algorithm (TDMA). Relaxation parameters and internal iterations for the variables were tuned to optimize the balance between the convergence criteria (1.0×10^{-3}) and the number of iterations required. The flow in bubble column was computed using grid size of $22 \times 62 \times 40$ (r, z, θ). The detailed stepwise procedure for getting the flow pattern is given by Ekambara and Joshi [8].

6.3. Connectivity between gas chamber and bubble column

The following stepwise procedure has been developed for describing the connectivity between the gas chamber and bubble column reactor.

(i) Initially, the gas chamber was simulated assuming uniform pressure on the downstream side equal to the static head of dispersion. The hole velocities through the distributor holes were calculated.
(ii) The hole velocities calculated from (i) were given to the bubble column as boundary conditions and the bubble column was simulated. As a result we get profiles of **u, v, w,** p, k and ε in the bubble column. The gas phase material balance was established while giving hole velocities to the bubble column. This step gives the pressure field in the entire column including that on the downstream side of the sparger.
(iii) The pressure profile above the sparger obtained in step (ii) was given as a boundary condition to the gas chamber and with this change the hole velocities were calculated.
(iv) The procedure in steps (ii and iii) was repeated until all hole velocities coming out of the gas chamber in consecutive iteration was within 4%. The downstream pressure profile obtained from consecutive iterations was also imposed to have a limit of 4% standard deviation.

For satisfying the two criteria in (iv), about three to four iterations were needed. For instance, Fig. 2 shows results of four iterations for connectivity between the gas chamber and bubble column reactor in the form of prediction of hold-up profile at three H_D/D locations (0.2, 2.5 and 5) in the bubble column reactor. In the sparger region and little above it (0.2 and 2.5), the effect of gas distribution can be clearly seen and at $H_D/D = 5$, there is no significant change in hold-up profile. Parasu Veera and Joshi [9] have observed the same trend in their experiments. It can be seen from Fig. 2 that in the first iteration, where the condition of static pressure of the dispersion above the gas chamber exists, gives the relatively uniform distribution. However, as seen in Fig. 2 the uniformity decreases as the pressure profile from the bubble column applied on the gas distributor above the gas chamber in consequently second and third iteration. No significant difference was observed between the third iteration and fourth iteration in this particular case. The hold-up profile results in a profile of static pressure, which is lower in the central region as compared to the near wall region. As a consequence, intense liquid circulation is a developed which is upwards in the central region and downward near the column wall. The intensity of liquid circulation depends upto the nature of hold-up profile. In case of a flat profile, the liquid circulation is zero. The circulation velocity increases with an increase in the steepness of the profile.

7. Results and discussion

7.1. Comparison of the flow pattern with the experimental data

As a first step, it is important to establish the validity of the model for flow pattern. Therefore, comparison has been made with the experimental data of Hills [10], Nottenkamper et al. [11], Menzel et al. [12], Yao et al. [13], Yu and Kim [14] and Grienberger and Hofmann [15]. The sparger

Table 2
Effect of the opening area, $D = 0.2$ m, $V_G = 0.1$ m s^{-1}, $H_D/D = 6$, $H_C/D = 1$, $d_0 = 2$ mm

% OA	No. of holes	Nozzle size (m)	V_N (m s^{-1})	ΔP_W (N m^{-2})	ΔP_D (N m^{-2})	Kinetic energy head	$^*R_1$	R_2	% S.D. with respect to mean
0.64	64	0.016	15.63	895.41	441.16	149.9	2.03	2.94	15.2
4.0	400	0.016	15.63	192.68	35.72	149.9	5.32	0.23	32.2

$^*R_1$ = Ratio of ΔP_W to ΔP_D, R_2 = ratio of ΔP_D to kinetic energy head.

Table 3
Effect of the hole size, $D = 0.2$ m, $V_G = 0.1$ m s^{-1}, $V_N = 15.625$ m s^{-1}, % OA ~ 0.64, $H_D/D = 6$, $H_C/D = 1$

N	d_0 (m)	Nozzle size (m)	ΔP_W (N m^{-2})	ΔP_D (N m^{-2})	Kinetic energy head	$^*R_1$	R_2	% S.D. with respect to mean
64	0.002	0.016	895.41	441.16	149.9	2.03	2.94	15.2
16	0.004	0.016	1090.8	299.98	149.9	3.63	2.01	25.1

$^*R_1$ = Ratio of ΔP_W to ΔP_D, R_2 = ratio of ΔP_D to kinetic energy head.

Table 4
Effect of the nozzle size, $D = 0.2$ m, $V_G = 0.1$ m s^{-1}, $d_0 = 2$ mm, $H_D/D = 6$, $N = 64$, $H_C/D = 1$, % OA = 0.64

Nozzle size (m)	V_N (m s^{-1})	ΔP_W (N m^{-2})	ΔP_D (N m^{-2})	Kinetic energy head	$^*R_1$	R_2	% S.D. with respect to mean
0.016	15.63	895.41	441.16	149.9	2.03	2.94	15.2
0.032	3.902	895.41	441.16	149.9	2.03	47.80	7.25
0.048	1.736	895.41	441.16	149.9	2.03	238.3	1.86

$^*R_1$ = Ratio of ΔP_W to ΔP_D, R_2 = ratio of ΔP_D to kinetic energy head.

Table 5
Effect of inlet position to the gas chamber for % OA = 0.64, $D = 0.2$ m, $N = 64$, $V_G = 0.1$ m s^{-1}, $d_0 = 2$ mm, $H_D/D = 6$, $H_C/D = 1$, $D_N = 16$ mm, $V_N = 15.625$ m s^{-1}

Position	ΔP_W (N m^{-2})	ΔP_D (N m^{-2})	Kinetic energy head	$^*R_1$	R_2	% S.D. with respect to mean
Center	895.41	441.16	149.9	2.03	2.94	15.20
Side nozzle at 1	895.41	441.16	149.9	2.03	2.94	4.07
Side nozzle at 2	895.41	441.16	149.9	2.03	2.94	3.02
Side nozzle at 3	895.41	441.16	149.9	2.03	2.94	27.45

$^*R_1$ = Ratio of ΔP_W to ΔP_D, R_2 = ratio of ΔP_D to kinetic energy head.

design was included in the simulation. Excellent comparison was obtained between the model predictions and the experimental data. For instance, Fig. 3 shows a typical case of such comparison. The agreement between the predicted and the experimental profiles of axial velocity can be seen to be excellent. It may be pointed out that such an agreement has been obtained over a wide range of column diameter, superficial gas and liquid velocities as covered by the above-mentioned authors. In view of the excellent comparison, it was thought desirable to simulate the effect of various chamber configurations on the flow pattern. For this purpose, a large number of sieve plate designs and the chamber configurations were selected. A summary of these plate-chamber configurations is given in Tables 2–6.

It is known that the uniformity of sparging increases with an increase in sparger pressure drop (ΔP_W) as compared with the static head of gas–liquid dispersion ($H_D \rho_D g$). However, an increase in the sparger pressure drop means an increase in the compressor (fixed) and compression (operating) costs. Therefore, it was thought desirable to seek the possibility of an optimum design.

7.2. CFD simulation for optimum design of gas distributor and gas chamber

The design procedure for distributors on the basis of CFD simulation of flow patterns in a combined coupled system consisting of a gas chamber, a bubble column and a sieve plate type

Table 6
Effect of height to width ratio for % OA = 0.64, $V_G = 0.1$ m s^{-1}, $V_N = 15.625$ m s^{-1}, $d_0 = 2$ mm, $D_N = 16$ mm, $N = 64$, $H_D/D = 6$

H_C/D	ΔP_W (N m^{-2})	ΔP_D (N m^{-2})	Kinetic energy head	$^*R_1$	R_2	% S.D. with respect to mean
2.0	946.41	268.34	149.9	2.03	1.80	2.10
1.5	924.90	445.74	149.9	2.03	1.74	4.60
1.0	895.41	441.32	149.9	2.03	2.94	15.20

$^*R_1$ = Ratio of ΔP_W to ΔP_D, R_2 = ratio of ΔP_D to kinetic energy head.

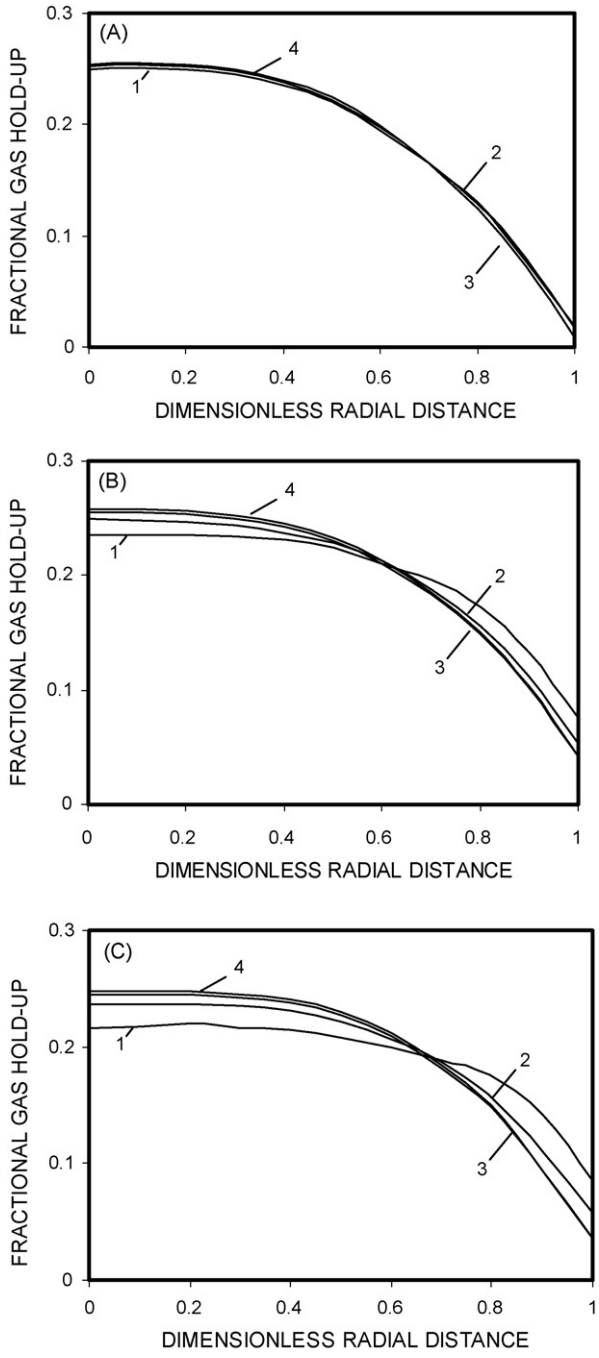

Fig. 2. Connectivity results for effect of pressure profile applied on the distributor plate ($d_0 = 2$ mm, $V_G = 0.1$ m s^{-1}, $N = 64$, $V_N = 15.25$ m s^{-1}, $D_N = 16$ mm (1, 2, 3, 4: first, second, third and fourth iteration results). (A) $H_C/D = 0.2$ (B) $H_C/D = 2.5$ (C) $H_C/D = 5.0$).

of gas distributor is as follows: (i) for a given pressure drop, selection of the opening area and the selection of hole size for maximum uniformity; (ii) for selected opening area and hole size, selection of nozzle size for maximum uniformity; (iii) for selected opening area, hole size, nozzle size, selection of position of inlet nozzle and aspect ratio of gas chamber. Finally (iv) optimization of pressure drop. The following study of effect of different design parameters will help in selecting proper parameter in step (i–iii).

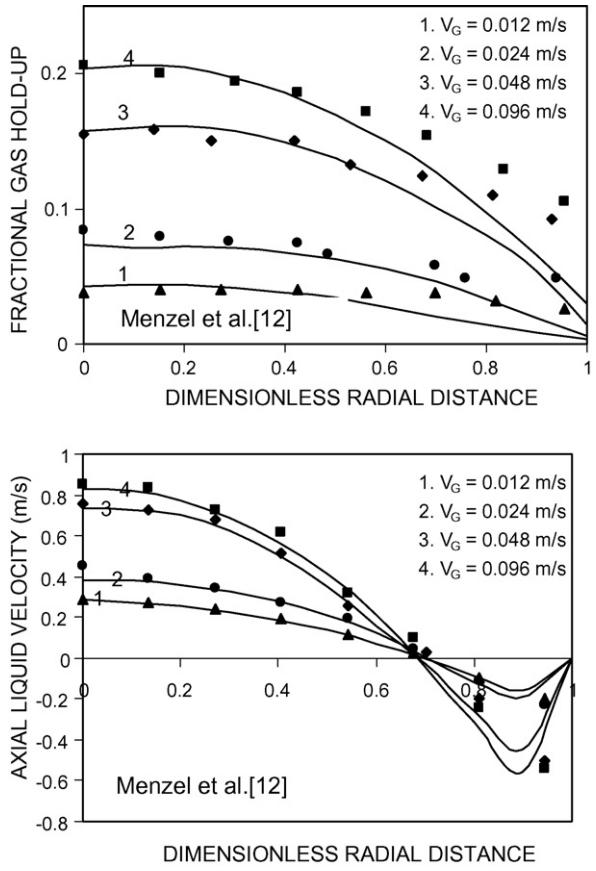

Fig. 3. Comparison of model prediction with the experimental data.

7.3. Effect of opening area

The simulations have been carried out for two extreme cases having low (0.64%) and high (4%) opening areas with corresponding 64 and 400 number of holes of 2 mm diameter. It was observed that when the opening area increases from 0.64 to 4%, a significant decrease in the uniformity occurs in the magnitude of the hole velocities. The effect of percentage opening area has been shown in Fig. 4 and Table 2. The average hold-up ($\bar{\in}_G$) decreases as the opening area increases. This is in agreement with the fact that with an increase in opening area, the distributor pressure drops decrease and the uniformity of pressure below the distributor decreases. The details regarding uniformity and pressure drop for the sparger considered are given in Table 2.

7.4. Effect of hole size

The hole size is an important parameter in design of the sparger. The effect of hole size has been shown in Fig. 5 and Table 3. Simulations have been carried out for hole sizes of 2 and 4 mm for 64 and 16 number of holes, respectively, with constant opening area of 0.64%. It can be seen from Table 3 that as the hole size increases, the pressure drop across the distributor decreases and the uniformity of distribution through the holes decreases. It was observed that in the sparger region and little above it ($H_D/D = 0.2$ and 2.5), the effect of gas distribution is significant. For 4 mm hole size, the hold-up profile is found to

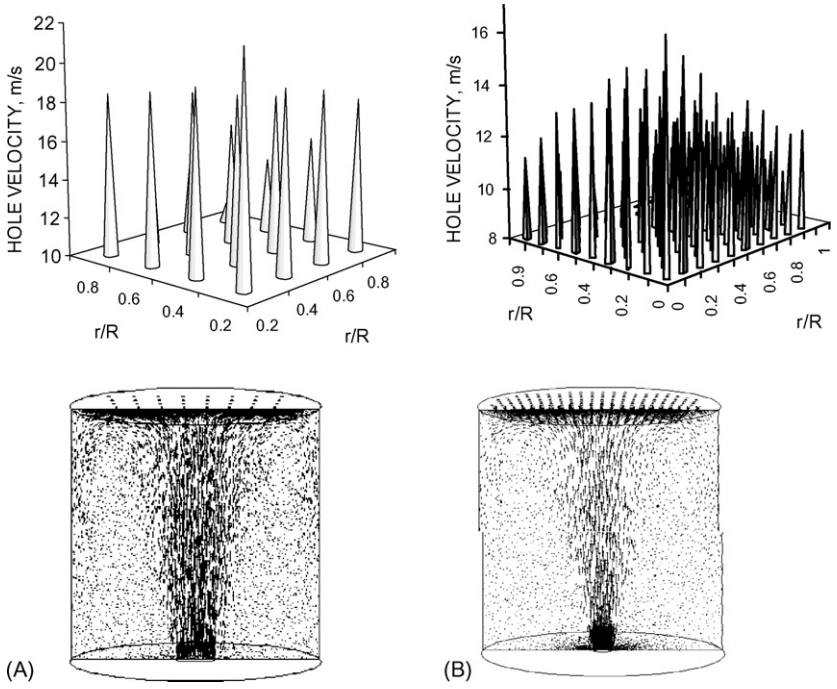

Fig. 4. Effect of percentage opening area on the gas distribution over the distributor plate and the flow pattern inside the gas chamber ($d_0 = 2$ mm, $V_G = 0.1$ m s^{-1}, $V_N = 15.25$ m s^{-1}, $D_N = 16$ mm and % opening area and number of holes of (A) 0.64 and 6 and (B) 4 and 400).

be steep at $H_D/D = 0.2$ and for 2 mm size for the same opening area, uniform distribution of gas occurs giving a relatively flat gas hold-up profile indicating the uniform distribution of the gas. Further, it was observed that as hole diameter increases the average hold-up ($\bar{\in}_G$) decreases. This can be attributed to the reduction in bubble size with a decrease in hole diameter and increases in the energy dissipation rate. Smaller bubble size results into the higher hold-up.

7.5. Effect of nozzle size

In the previous two sections, it was observed that the uniformity of distribution increases with an increase in the distributor pressure drop. In this context, for a given distributor pressure drop, it was thought desirable to investigate the effect of inlet nozzle size. This is because the kinetic head of the inlet gas ($V_N^2/2$) is expected to have implications on the gas distribu-

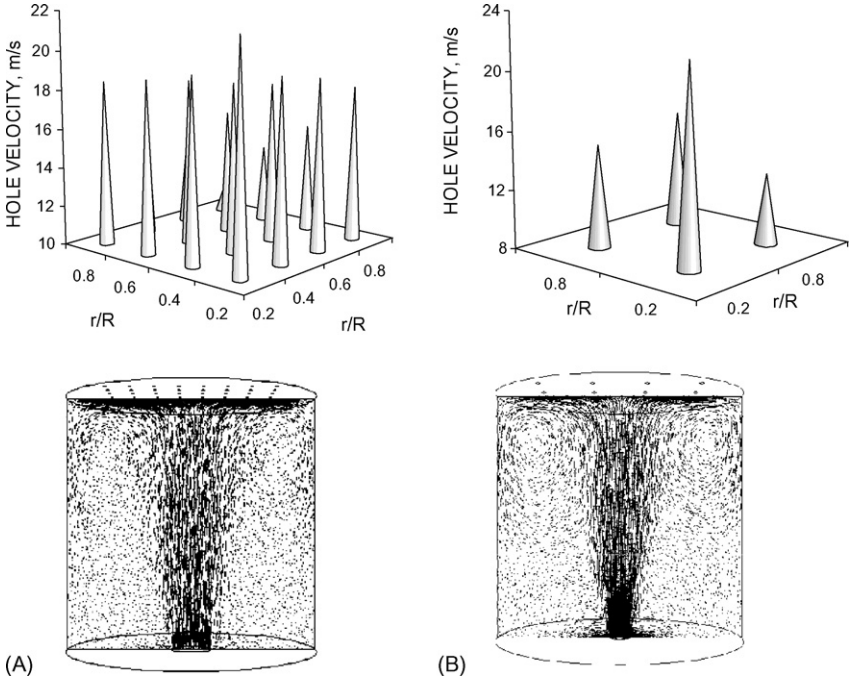

Fig. 5. Effect of hole size on the gas distribution over the distributor plate and the flow pattern inside the gas chamber (% OA ~ 0.64, $V_G = 0.1$ m s^{-1}, $V_N = 15.25$ m s^{-1}, $D_N = 16$ mm, N and d_0 of (A) 64 and 2 mm and (B) 16 and 4 mm).

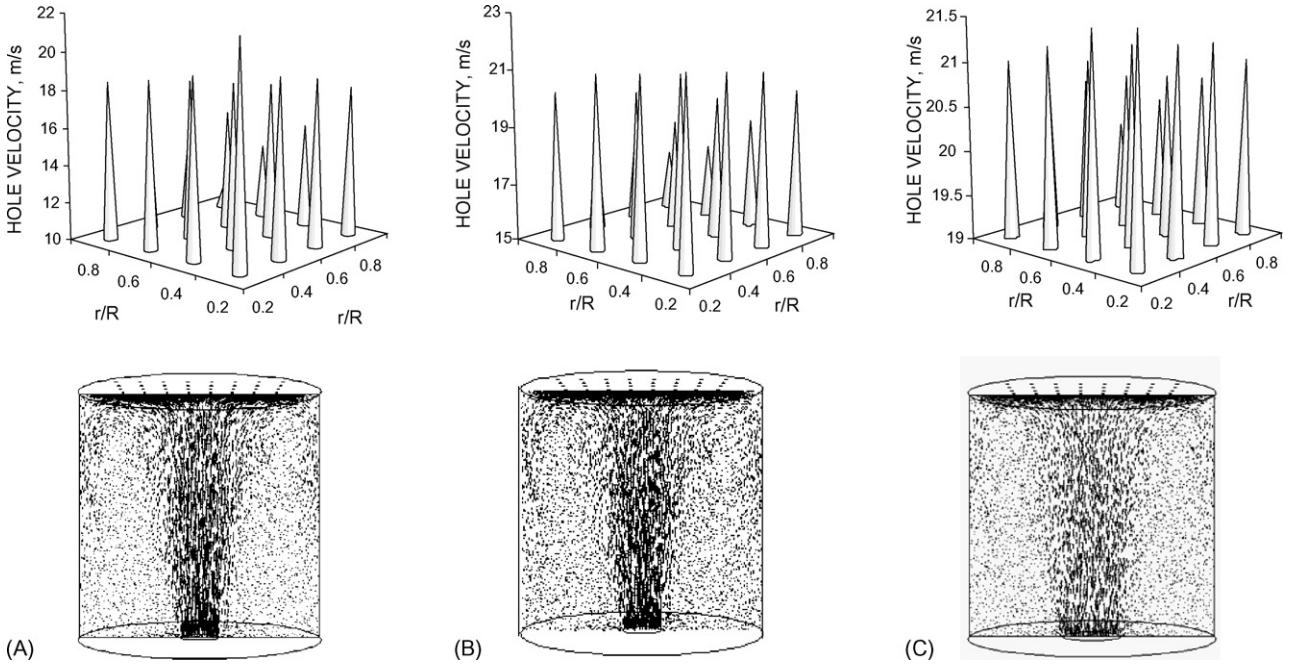

Fig. 6. Effect of nozzle size on the gas distribution over the distributor plate and the flow pattern inside the gas chamber ($d_0 = 2$ mm, $V_G = 0.1$ m s^{-1}, $N = 64$, % OA = 0.64 and V_N, D_N of (A) 15.6 m s^{-1}, 16 mm; (B) 3.9 m s^{-1}, 32 mm; (C) 1.7 m s^{-1}, 48 mm).

tion. It can be seen that, for a given distributor pressure drop; a decrease in the kinetic head improves the uniformity. For this purpose, the distributor having 64 holes was selected and simulated for three different nozzle size (16, 32, 48 mm). It can be seen from Fig. 6 and Table 4 that for case one, where kinetic head is high as compared to rest, gives non-uniform distribution of the gas.

7.6. Effect of inlet nozzle position

As seen in the earlier section, nozzle size plays a significant role in deciding uniformity. Therefore, it was thought desirable to see the effect of nozzle position on the flow pattern in the bubble column. The simulations have been carried out by keeping the inlet nozzle location at four different positions: (i) on the center of the bottom and (ii) on the side at three different positions (top, center and bottom). The effect of the inlet nozzle position is shown in Fig. 7 and Table 5. It can be seen that the side central and side bottom position gives relatively better uniformity as compared to the bottom central position and top positions. Fig. 7 shows the effect of these configurations on the bubble column, it was observed that the side central position and side bottom give a relatively flat hold-up profile, more so than side upper and bottom and central position.

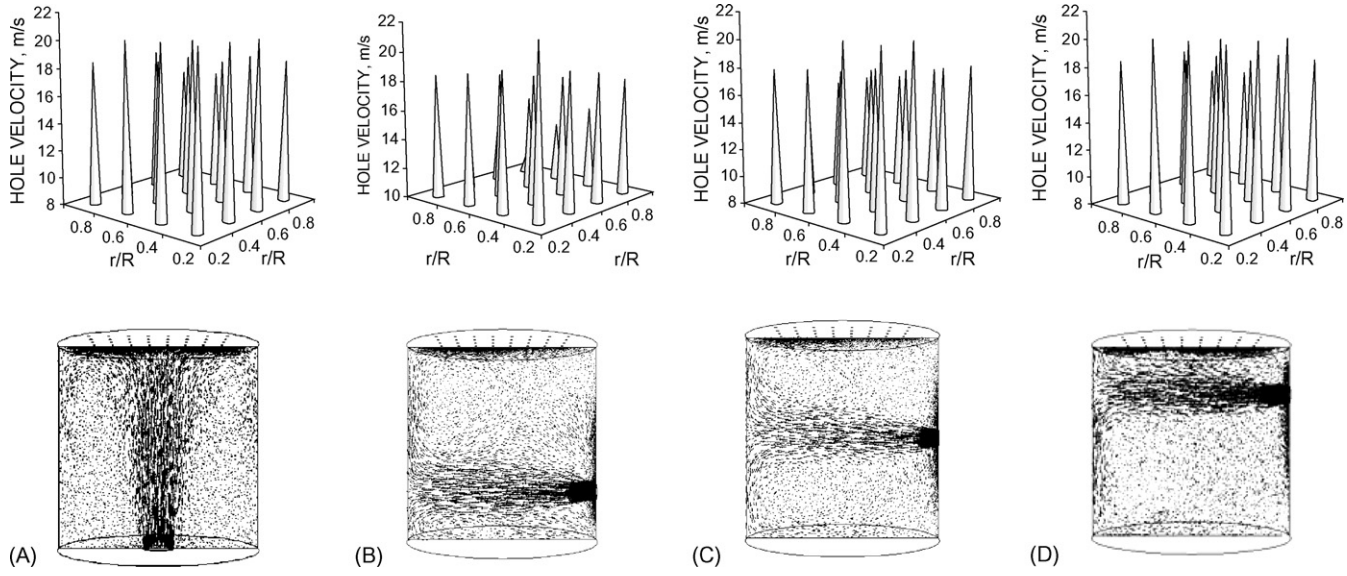

Fig. 7. Effect of inlet position on the nozzle on the gas distribution over the distributor plate and the flow pattern inside the gas chamber (% OA = 0.64, $N = 64$, $H_C/D = 1$, $d_0 = 2$ mm, $D_N = 16$ mm, $V_G = 0.1$ m s^{-1}, $V_N = 15.25$ m s^{-1} and with inlet nozzle positions of (A) center at the bottom; (B) side at the bottom; (C) side at center; (D) side at top).

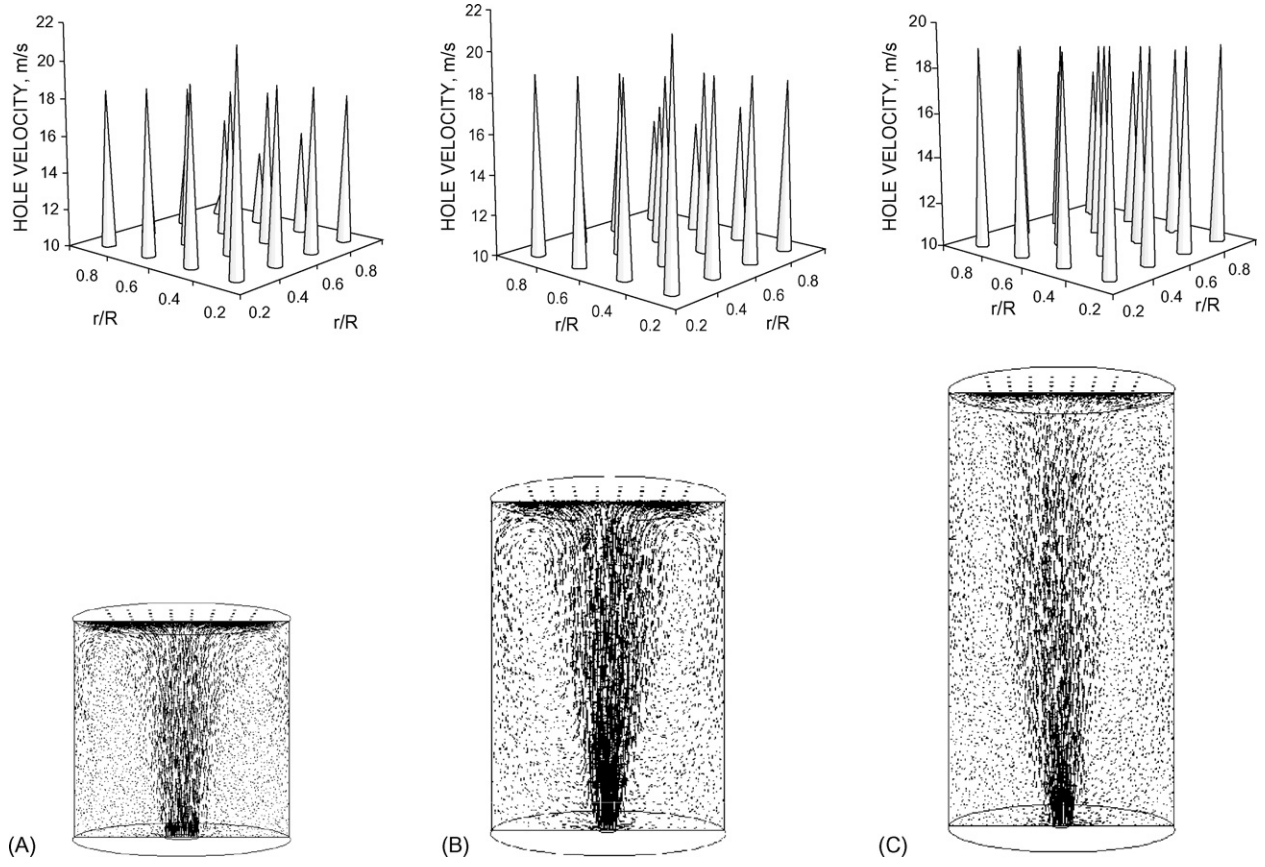

Fig. 8. Effect of height to diameter ratio on the gas distribution over the distributor plate and the flow pattern inside the gas chamber ($V_G = 0.1\ m\ s^{-1}$, $V_N = 15.25\ m\ s^{-1}$, % OA = 0.64, $N = 64$, $d_0 = 2$ mm, $D_N = 16$ mm and H_C/D of (A) 1; (B) 1.5; (C) 2).

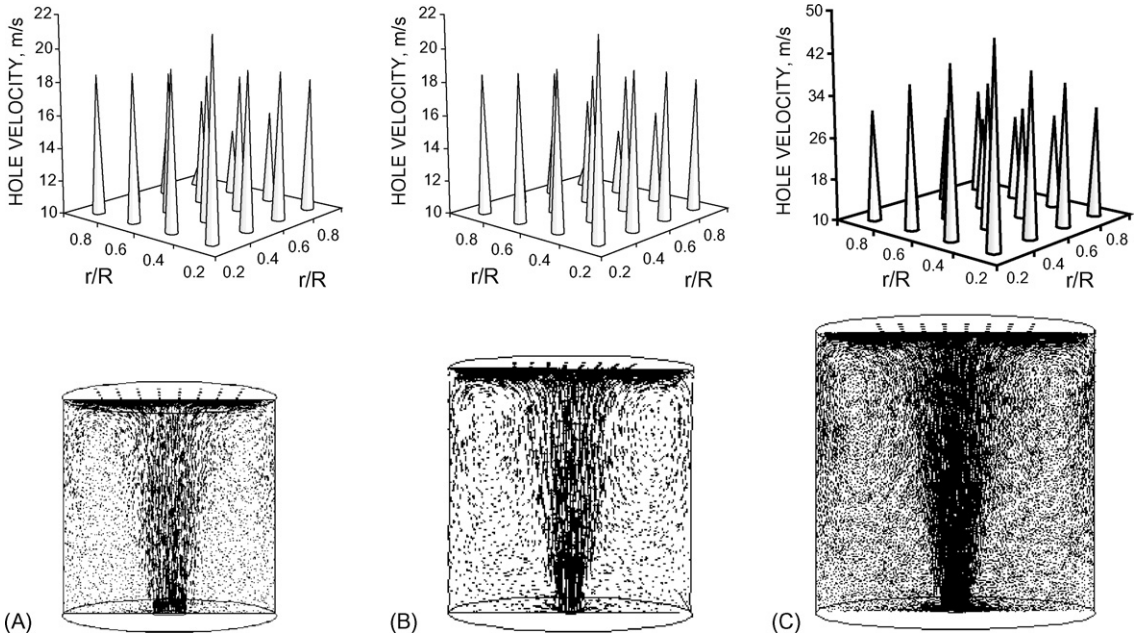

Fig. 9. Effect of column diameter (D) on the gas distribution over the distributor plate and the flow pattern inside the gas chamber ($V_G = 0.1\ m\ s^{-1}$, $V_N = 15.25\ m\ s^{-1}$, % OA = 0.64, $N = 64$, $d_0 = 2$ mm, $H_C/D = 1$ and the column diameter (D) of (A) 0.2 m; (B) 0.3 m; (C) 0.4 m).

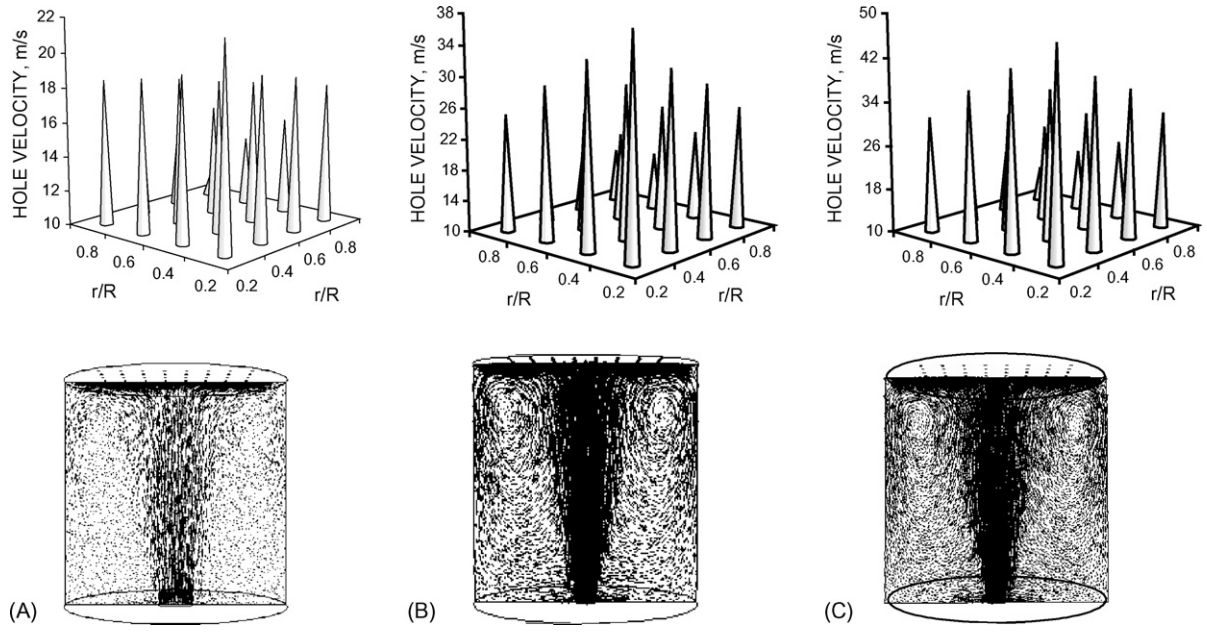

Fig. 10. Effect of superficial gas velocity on the gas distribution over the distributor plate and the flow pattern inside the gas chamber ($D = 0.2$ m, % OA = 0.64, $N = 64$, $d_0 = 2$ mm, $D_N = 16$ mm and V_G of (A) 0.1 m s^{-1}; (B) 0.2 m s^{-1}; (C) 0.25 m s^{-1}.

7.7. Effect of aspect ratio of gas chamber

The simulations have been carried out by changing the height of the chamber (0.2, 0.3, 0.4 m). As expected, the uniformity increases with an increase in the height to diameter ratio. As height to diameter ratio increases from 1 to 2, the main stream of the air takes time to reach the distributor and dissipates itself before reaching the central portion of the distributor. As a result for the height of 0.4 m, air enters the chamber and while reaching to the distributor, it spreads out and achieves the significant degree of uniformity and reduces the mal-distribution. It was observed that in the sparger region and little above it ($H_D/D = 0.2$ and 2.5), effect on gas distribution was significant. Fig. 8 and Table 6 shows the effect of height of the chamber on the hydrodynamics of the bubble column. It was observed that at height of 0.4 m, relatively flat hold-up profile as compared to the other two cases of 0.2 and 0.3 m.

7.8. Effect of column diameter

The simulations have been carried out to see the effect of the column diameter and hence the chamber diameter (0.2, 0.3, 0.4, 0.6 m), keeping the percentage opening area constant. It was observed that as column diameter increases, mal-distribution over the distributor increases. Further, it was found that the resulting hold-up profile shows little variation with change in column diameter (0.2–0.6 m), indicating the hold-up profile is independent of column diameter. The effect of column diameter has been shown in Fig. 9 and Table 7.

7.9. Effect of superficial gas velocity

The simulations have been carried out for the superficial gas velocity of 0.1, 0.2, 0.25 m s^{-1}. The effect of superficial gas velocity on the flow pattern in the chamber is illustrated in Fig. 10 and Table 8. It can be seen that as superficial gas velocity increases, mal-distribution over the distributor increases.

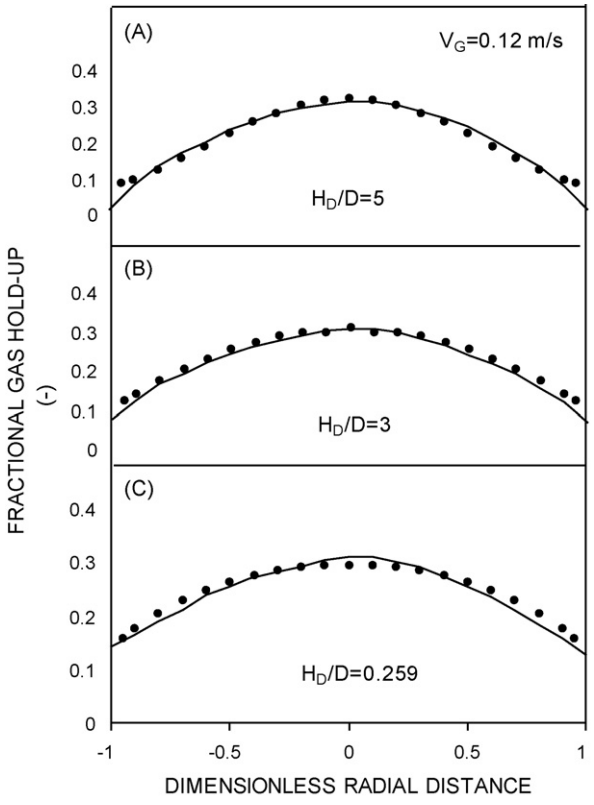

Fig. 11. Comparison of hold-up at height to diameter ratio of (A) 5; (B) 3; (C) 0.259 with the experimental data of Parasu Veera and Joshi [9] ($D = 0.385$ m, % OA = 0.44, $N = 71$, $V_G = 0.12$ m s^{-1}).

Table 7
Effect of column diameter for % OA = 0.64, $V_G = 0.1\ m\ s^{-1}$, $V_N = 15.625\ m\ s^{-1}$, $N = 64$, $H_D/D = 6$

Diameter (m)	d_0 (mm)	ΔP_W (N m^{-2})	ΔP_D (N m^{-2})	Kinetic energy head	$^*R_1$	R_2	% S.D. with respect to mean
0.2	2	895.41	441.16	149.9	2.03	2.94	15.2
0.3	4	413.4	262.90	149.9	1.57	1.69	18.5
0.4	4	384.5	269.03	149.9	1.42	1.75	20.4
0.6	4	357.4	277.90	149.9	1.29	1.85	25.2

$^*R_1$ = Ratio of ΔP_W to ΔP_D, R_2 = ratio of ΔP_D to kinetic energy head.

Table 8
Effect of superficial gas velocity for % OA = 0.64, $N = 64$, $H_D/D = 6$, $D = 0.2$ m

V_G	Hole size (mm)	ΔP_W (N m^{-2})	ΔP_D (N m^{-2})	Kinetic energy head	$^*R_1$	R_2	% S.D. with respect to mean
0.1	2	895.41	441.16	149.9	2.03	2.94	15.20
0.2	2	635.25	1187.98	599.60	1.87	1.05	23.25
0.25	2	1546.65	855.918	936.89	1.80	0.913	26.45

$^*R_1$ = Ratio of ΔP_W to ΔP_D, R_2 = ratio of ΔP_D to kinetic energy head.

8. Development of hold-up profile and its significance

The establishment of the flow pattern in the column is an effect of the synchronized development in the gas hold-up profile and also the liquid circulation. Thus, in the heterogeneous regime of operation ($d_0 > 1.9$ mm and $V_G > 50\ mm\ s^{-1}$), the circulation velocity increases continuously away from the sparger, resulting more bubbles being brought into the center, thus helping the development of the hold-up profile as well. The development of the hold-up profile for different spargers (SP1–SP6, details are given in Table 9) is shown in Figs. 11 and 12 for the air–water system. Fig. 11 shows that the comparison of hold-up profile with the experimental data of Parasu Veera and Joshi [9] for a superficial gas velocity of $0.12\ m\ s^{-1}$. It can be seen that the profile is relatively flatter at the H_D/D ratio of 0.259 and the centerline hold-up increases with an increase in the height from the sparger. As a result, the driving force for the liquid circulation, $\Delta \in_G$ (the difference between the centerline hold-up and the wall

Table 9
Details of the sparger used

Sparger	Specification
SP1	% OA = 0.64, $N = 64$, $d_0 = 2$ mm, $D = 0.2$
SP2	% OA = 4.0, $N = 400$, $d_0 = 2$ mm, $D = 0.2$
SP3	% OA = 0.64, $N = 16$, $d_0 = 4$ mm, $D = 0.2$
SP4	% OA = 0.64, $N = 64$, $d_0 = 3$ mm, $D = 0.3$
SP5	% OA = 0.64, $N = 64$, $d_0 = 4$ mm, $D = 0.4$
SP6	% OA = 0.42, $N = 71$, $d_0 = 3$ mm, $D = 0.385$

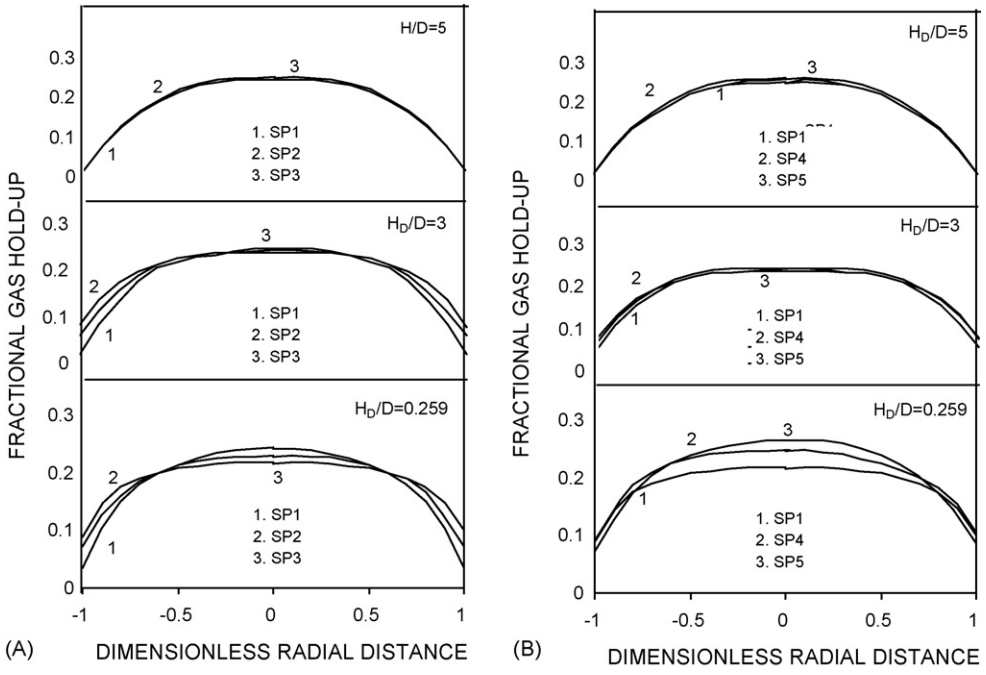

Fig. 12. (A and B) Development of hold-up profile for various spargers of the configuration (SP1 (% OA = 0.64, $N = 64$, $d_0 = 2$ mm, $D = 0.2$), SP2 (% OA = 4.0, $N = 400$, $d_0 = 2$ mm, $D = 0.2$), SP3 (% OA = 0.64, $N = 16$, $d_0 = 4$ mm, $D = 0.2$), SP4 (% OA = 0.64, $N = 64$, $d_0 = 3$ mm, $D = 0.3$), SP5 (% OA = 0.64, $N = 64$, $d_0 = 4$ mm, $D = 0.4$).

Table 10
Comparison of mixing time with experimental data at different H_D/D

$D = 0.2$ m		H_D/D							
V_G (m s^{-1})	$\bar{\epsilon}_G$	3		5		8		10	
		Experimental θ_{mix}	CFD θ_{mix}	Experimental θ_{mix}	CFD θ_{mix}	Experimental θ_{mix}	CFD θ_{mix}	Experimental θ_{mix}	CFD θ_{mix}
0.070	0.135	33.5	36.8	38.4	43.1	51.6	54.3	72.5	77.7
0.170	0.223	29.3	33.1	35.2	41.2	45.6	50.8	67.2	72.4
0.295	0.282	25.2	28.5	31.2	33.6	39.6	44.3	–	66.3
$D = 0.4$ m		H_D/D							
V_G (m s^{-1})	$\bar{\epsilon}_G$	2		3		4		5	
		Experimental θ_{mix}	CFD θ_{mix}	Experimental θ_{mix}	CFD θ_{mix}	Experimental θ_{mix}	CFD θ_{mix}	Experimental θ_{mix}	CFD θ_{mix}
0.070	0.135	56.5	61.1	66.0	69.1	78.0	81.9	88.0	90.3
0.170	0.223	51.6	53.0	61.2	64.7	71.5	75.4	79.5	83.8
0.295	0.282	47.0	50.8	55.5	57.8	64.0	66.2	–	71.4

hold-up) increases as the distance increases from the sparger up to a H_D/D value of 5. The contribution of liquid circulation on the development of the hold-up profile can be explained as the liquid circulation and the gas hold-up profile are strongly interrelated and develop together. The liquid circulation is upward where the gas hold-up is greater, especially in the central region of the column. Therefore, the overall bubble rise velocity is higher in the central region where the gas concentration is also high. As the result, the liquid circulation reduces the residence time of the gas phase and hence the value of $\bar{\epsilon}_G$ decreases with an increase in the H_D/D ratio.

In view of the success of the model to predict the hold-up profile accurately at different height to diameter ratios, it was thought desirable to see its effect on design objectives like mixing time, interfacial area and mass transfer coefficient. For the prediction of mixing time, the methodology developed by Ekambara and Joshi [8] has been employed. The effect of H_D/D ratio on mixing time was studied in 0.2 and 0.4 m i.d. column with variation in V_G from 0.07 to 0.295 m s^{-1}. For 0.2 m i.d. column the H_D/D ratio was varied from 3 to 10; and from 2 to 5 for a 0.4 m i.d. column, respectively. Comparison of the predicted and the experimental data of the mixing time (θ_{mix}) for different H_D/D are given in Table 10. It can be seen that the mixing time increases with an increase in H_D/D ratio for both the columns. Also, it can be noted that at same H_D/D the mixing time increases with an increase in column diameter (D). The effect of height to diameter ratio (1–10) on the axial dispersion coefficient was studied for column diameters 0.2 and 0.4 m. The CFD predictions of the axial dispersion coefficient are given in Table 11. It can be seen from the table that the axial dispersion coefficient increases with an increase H_D/D for both the column. Akita and Yoshida [16] have reported the mass transfer coefficient to be proportional to $\bar{\epsilon}_G^{1.1}$. More recently, Bando et al. [17] have reported systematic analysis of the effect of H_D/D on mass transfer coefficient using multi-point spargers. They observed that the mass transfer coefficient decreases with an increase in H_D/D. The CFD simulations for superficial gas velocity of 0.1 m s^{-1} for the 0.2 m diameter column for different multi-point sparger (SP1–SP6) show that as H_D/D increases, the average hold-up decreases. Further, CFD predicted average hold-up was used in

Table 11
Comparison of axial dispersion coefficient with experimental data at different H_D/D

$D = 0.2$ m		H_D/D			
V_G (m s^{-1})	$\bar{\epsilon}_G$	Axial dispersion coefficient, D_L (m^2 s^{-1})			
		3	5	8	10
0.070	0.135	0.0071	0.0139	0.0208	0.0318
0.170	0.223	0.0155	0.0242	0.0292	0.0341
0.295	0.282	0.0221	0.0368	0.0436	0.0484
$D = 0.4$ m		H_D/D			
V_G (m s^{-1})	$\bar{\epsilon}_G$	Axial dispersion coefficient, D_L (m^2 s^{-1})			
		2	3	4	5
0.070	0.135	0.0188	0.0283	0.0417	0.0682
0.170	0.223	0.0371	0.0498	0.0706	0.0981
0.295	0.282	0.0382	0.0664	0.1004	0.1212

Table 12
Effect H_D/D on interfacial area and mass transfer coefficient

H_D/D	a (m^{-1})	k_La (s^{-1})
1	39.6491	0.002669
2	37.4164	0.0021622
3	33.2166	0.0018155
4	31.3461	0.0015785
5	29.5624	0.0014164
6	28.9724	0.0013055

the mass transfer correlations given by Akita and Yoshida [16]. The values of interfacial area and mass transfer coefficient are given in Table 12, and it can be seen that the trend obtained is in an agreement with observation that the mass transfer coefficient decreases with an increase in H_D/D. The foregoing discussions on the effect of sparger design and the H_D/D on mixing time, dispersion coefficient, mass transfer coefficient supports the CFD model developed in this work for a combined system of bubble column (with different H_D/D), sparger and the gas chamber of various geometries.

9. Conclusion

A three-dimensional CFD model has been developed for a combined system consisting of gas chamber, sparger and a column. The gas chamber together with sieve plate sparger were simulated using FLUENT, while the bubble column has been simulated using an in-house CFD code. A systematic procedure has been developed to understand the effects of various chamber configurations on the performance of a bubble column. It was found that, the chamber configuration has an effect on the quality of gas distribution particularly in the sparger region ($H_D/D < 5$) of the bubble column. The uniformity of gas distribution was found to increase with an increase in the distributor pressure drop and a decrease in the inlet kinetic head of the gas. From the quantitative information reported in this paper, it may be possible to select the design parameters of distributor and gas chamber depending upon the desired level of uniformity of distribution.

Acknowledgement

One of us (Mahesh T. Dhotre) acknowledges the fellowship support given by the University Grants Commission (UGC), Government of India.

References

[1] D. Kunii, O. Levenspiel, Fluidization Engineering, second ed., Butterworth-Heinemann, London, 1991.
[2] M.T. Dhotre, J.B. Joshi, CFD simulation of gas chamber for gas distributor design, Can. J. Chem. Eng. 81 (2003) 677–683.
[3] H.B. Stewart, B. Wendroff, Two-phase flow: models and methods, J. Comp. Phys. 56 (1984) 363–409.
[4] H.A. Jakobsen, B.H. Sannaes, S. Grevskott, H.F. Svendsen, Modelling of vertical bubble-driven flows, Ind. Eng. Chem. Res. 36 (1997) 4052–4074.
[5] J.B. Joshi, Computational flow modelling and design of bubble column reactors, Chem. Eng. Sci. 56 (2001) 5893–5933.
[6] M.T. Dhotre, J.B. Joshi, Two dimensional CFD model for the prediction of flow pattern, pressure drop and heat transfer coefficient in bubble column reactors, Chem. Eng. Res. Des. 82 (2004) 689–707.
[7] S.V. Patankar, Numerical Heat Transfer and Fluid Flow, McGraw-Hill, New York, 1980.
[8] K. Ekambara, J.B. Joshi, CFD simulation of residence time distribution and mixing in bubble column reactors, Can. J. Chem. Eng. 81 (2003) 668–669.
[9] U. Parasu Veera, J.B. Joshi, Measurement of gas hold up profiles by gamma ray tomography: effect of sparger design and height of dispersion in bubble columns, Chem. Eng. Res. Des. 77 (1999) 303–317.
[10] J.H. Hills, Radial non-uniformity of velocity and voidage in a bubble column, Trans. IchemE. 52 (1974) 1–9.
[11] R. Nottenkamper, A. Stieff, P.M. Weinspach, Experimental investigations of hydrodynamics of bubble columns, Ger. Chem. Eng. 6 (1983) 147–155.
[12] T. Menzel, T. Weide, O. Staudacher, O. Wein, U. Onken, Reynolds shear stress for modelling of bubble column reactor, Ind. Eng. Chem. Res. 29 (1990) 988–994.
[13] B.P. Yao, C. Zheng, H.E. Gasche, H. Hofmann, Bubble behaviour and flow structure of bubble columns, Chem. Eng. Proc. 29 (1991) 65–75.
[14] Y.H. Yu, S.D. Kim, Bubble properties and local liquid velocity in the radial direction of co-current gas–liquid flow, Chem. Eng. Sci. 46 (1991) 313–332.
[15] J. Grienberger, H. Hofmann, Investigation and modeling of bubble columns, Chem. Eng. Sci. 47 (1992) 2215–2220.
[16] K. Akita, F. Yoshida, Bubble size, interfacial area and liquid-phase mass transfer coefficient in bubble columns, Ind. Eng. Chem. Pro. Dev. Des. 13 (1974) 84.
[17] Y. Bando, M. Chaya, S. Hamano, K. Yasuda, M. Nakamura, K. Osada, M. Matsui, Effect of liquid height on flow characteristics in bubble column using highly viscous liquid, J. Chem. Eng. Jpn. 36 (5) (2003) 523.